

Pasta phases within the QMC model

Guilherme Grams¹, Alexandre M. Santos¹, Prafulla K. Panda², Constança Providência³, Débora P. Menezes¹

¹*Depto de Física, CFM, Universidade Federal de Santa Catarina, Brazil*

²*Department of Physics, Utkal University, Bhubaneswar-751 004, India*

³*CFisUC, Department of Physics, University of Coimbra, P-3004-516 Coimbra, Portugal*

In this work the low density regions of nuclear and neutron star matter are studied. The search for the existence of pasta phases in this region is performed within the context of the quark-meson coupling (QMC) model, which incorporates quark degrees of freedom. Fixed proton fractions are considered, as well as nuclear matter in beta equilibrium at zero temperature. We discuss the recent attempts to better understand the surface energy in the coexistence phases regime and we present results that show the existence of the pasta phases subject to some choices of the surface energy coefficient. We also analyze the influence of the nuclear pasta on some neutron star properties. The equation of state containing the pasta phase will be part of a complete grid for future use in supernova simulations.

PACS numbers: 26.60.Kp, 26.50.+x, 95.30.Tg, 24.10.Jv

I. INTRODUCTION

At very low nuclear matter density, a competition between the strong and the electromagnetic interactions takes place [1, 2], leading to a configuration in which its free energy per particle may be lower than the corresponding to the homogeneous phase at the same density. The so-called *pasta phases* are therefore the preferred shapes of some systems at these densities [3–6]. These structures look like droplets, bubbles, rods, tubes and slabs [3], and are expected to exist [7, 8] both in the crust of neutron stars (zero temperature, very low proton fraction, matter in β -equilibrium) and in supernova (finite temperature, proton fraction around 0.3).

From the analysis of glitches, the authors of [9] have related the fraction of the moment of inertia contained in the crust of the Vela pulsar with the mass and the radius of the neutron star and the pressure and density at the crust-core interface. From realistic EoS they have obtained an expected range of values for the pressure at the inner edge of the crust and therefore also a relation between the radius and mass of the pulsar. This work shows the importance of understanding the exact density limits of the pasta phases and its consequences on the choice of appropriate equations of state. More recently, the existence of the pasta phase in the neutron star crust was shown to considerably alter the neutrino mean-free paths and its diffusion coefficients as compared with the homogeneous matter results. The consequent differences in neutrino opacities certainly influence the Kelvin-Helmholtz phase of the star evolution [10, 11].

On the other hand, due to well known observational difficulties, simulations of core-collapse supernova have played an important role in the study of supernovae explosions and the evolution of their possible remnants. Hence, obtaining appropriate equations of state (EoS) for core-collapse supernova simulations has been a very challenging task. For this class of EoS one needs a grid of thermodynamic quantities with densities ranging from 10^5 to more than 10^{15} g.cm⁻³, proton fractions up to

about 0.6 and temperatures varying from zero to more than 100 MeV. So far, in the models used for the obtention of a complete grid with the aim of being tested in supernova simulations, inhomogeneous matter believed to be present at low densities, has only been considered with the inclusion of clusters [12–16]. However, according to the works of [17, 18] the pasta phases may form 10 – 20% of the mass of the supernova core, therefore its role should not be disregarded. The pasta phases have been studied in the context of several models [1, 18–21] and all of them predict its existence under the conditions expected to be found in the inner crust of compact objects, although the profiles show that they vary in many aspects [8, 19].

The quark meson coupling (QMC) model [22–24] describes nuclear matter as a system of non-overlapping MIT-like bags, interacting with each other by interchanging meson fields. Hence, it contains more fundamental degrees of freedom than the usual quantum hydrodynamic models, so far used to the study of the pasta phases [1, 10, 19, 25]. With the aim of constructing a complete grid for supernova simulations, a preliminary work at zero temperature, $\rho = 10^{14} - 10^{16}$ g.cm⁻³ and $Y_p = 0 - 0.65$ was done [26] and revealed that the QMC is a promising model.

In the present work, we study the possible existence of the pasta structures within the QMC model at zero temperature and its dependence on the surface energy coefficient. The work is organized as follows: In Sec. II the QMC model is briefly reviewed and the method of the coexisting phases used to build the pasta phase is presented in Sec. III, where a detailed study of the surface tension coefficient is performed. In Sec. IV we present our results and draw the conclusions. In the last Section, we make some final remarks.

II. THE QUARK-MESON COUPLING MODEL

In the QMC model, the nucleon in nuclear medium is assumed to be a static spherical MIT bag in which quarks interact with the scalar (σ) and vector (ω , ρ) fields, and those are treated as classical fields in the mean field approximation (MFA) [22]. The quark field, ψ_{qN} , inside the bag then satisfies the equation of motion:

$$\left[i \not{\partial} - (m_q^0 - g_\sigma^q) - g_\omega^q \omega \gamma^0 + \frac{1}{2} g_\rho^q \tau_z \rho_{03} \gamma^0 \right] \psi_{qN}(x) = 0, \quad q = u, d \quad (1)$$

where m_q^0 is the current quark mass, and g_σ^q , g_ω^q and g_ρ^q denote the quark-meson coupling constants. The normalized ground state for a quark in the bag is given by

$$\psi_{qN}(\mathbf{r}, t) = \mathcal{N}_{qN} \exp(-i\epsilon_{qN} t/R_N) \times \begin{pmatrix} j_{0N}(x_{qN} r/R_N) \\ i\beta_{qN} \vec{\sigma} \cdot \hat{r} j_{1N}(x_{qN} r/R_N) \end{pmatrix} \frac{\chi_q}{\sqrt{4\pi}}, \quad (2)$$

where

$$\epsilon_{qN} = \Omega_{qN} + R_N \left(g_\omega^q \omega + \frac{1}{2} g_\rho^q \tau_z \rho_{03} \right), \quad (3)$$

and,

$$\beta_{qN} = \sqrt{\frac{\Omega_{qN} - R_N m_q^*}{\Omega_{qN} + R_N m_q^*}}, \quad (4)$$

with the normalization factor given by

$$\mathcal{N}_{qN}^{-2} = 2R_N^3 j_0^2(x_q) [\Omega_q(\Omega_q - 1) + R_N m_q^*/2] / x_q^2, \quad (5)$$

where $\Omega_{qN} \equiv \sqrt{x_{qN}^2 + (R_N m_q^*)^2}$, $m_q^* = m_q^0 - g_\sigma^q \sigma$, R_N is the bag radius of nucleon N and χ_q is the quark spinor. The bag eigenvalue for nucleon N , x_{qN} , is determined by the boundary condition at the bag surface

$$j_{0N}(x_{qN}) = \beta_{qN} j_{1N}(x_{qN}). \quad (6)$$

The energy of a static bag describing nucleon N consisting of three quarks in ground state is expressed as

$$E_N^{\text{bag}} = \sum_q n_q \frac{\Omega_{qN}}{R_N} - \frac{Z_N}{R_N} + \frac{4}{3} \pi R_N^3 B_N, \quad (7)$$

where Z_N is a parameter which accounts for zero-point motion of nucleon N and B_N is the bag constant. The set of parameters used in the present work is determined by enforcing stability of the nucleon (here, the ‘‘bag’’), much like in [27], so there is a single value for proton and neutron masses. The effective mass of a nucleon bag at rest is taken to be $M_N^* = E_N^{\text{bag}}$.

The equilibrium condition for the bag is obtained by minimizing the effective mass, M_N^* with respect to the bag radius

$$\frac{dM_N^*}{dR_N} = 0, \quad N = p, n, \quad (8)$$

By fixing the bag radius $R_N = 0.6$ fm and the bare nucleon mass $M = 939$ MeV the unknowns $Z_N = 4.0050668$ and $B_N^{1/4} = 210.85$ MeV are then obtained. Furthermore, the desired values of $B/A \equiv \epsilon/\rho - M = -15.7$ MeV at saturation $n = n_0 = 0.15$ fm $^{-3}$, are achieved by setting $g_\sigma^q = 5.9810$, $g_\omega = 8.9817$, $g_\rho = 8.6510$, where $g_\omega = 3g_\sigma^q$ and $g_\rho = g_\rho^q$. The meson masses are $m_\sigma = 550$ MeV, $m_\omega = 783$ MeV and $m_\rho = 770$ MeV. With this parameterization, some of the bulk properties at saturation density are the compressibility, the symmetry energy and the slope of the symmetry energy, whose values can be seen in table I. These numbers are very close to the most accepted values (see [28], for instance) and J and L_0 can be easily controlled by the inclusion of a $\omega - \rho$ interaction, as discussed in [29–31]. The larger the value of this interaction, the lower the values of the symmetry energy and its slope. Other parameterizations are also possible. Of particular interest is the modified QMC model, where the parameters are adjusted so that the constituent quarks are confined to a flavour-independent potential where pionic and gluonic corrections are taken into account [32, 33]. These studies will be performed in future investigations. Within the parameterization we have chosen, the total energy density of the nuclear matter reads

$$\begin{aligned} \epsilon &= \frac{1}{2} m_\sigma^2 \sigma + \frac{1}{2} m_\omega^2 \omega_0^2 + \frac{1}{2} m_\rho^2 \rho_{03}^2 \\ &+ \sum_N \frac{1}{\pi^2} \int_0^{k_N} k^2 dk [k^2 + M_N^{*2}]^{1/2}, \end{aligned} \quad (9)$$

and the pressure is,

$$\begin{aligned} p &= -\frac{1}{2} m_\sigma^2 \sigma + \frac{1}{2} m_\omega^2 \omega_0^2 + \frac{1}{2} m_\rho^2 \rho_{03}^2 \\ &+ \sum_N \frac{1}{\pi^2} \int_0^{k_N} k^4 dk / [k^2 + M_N^{*2}]^{1/2}. \end{aligned} \quad (10)$$

The vector mean field ω_0 and ρ_{03} are determined through

$$\omega_0 = \frac{g_\omega(n_p + n_n)}{m_\omega^2}, \quad \rho_{03} = \frac{g_\rho(n_p - n_n)}{2m_\rho^2}, \quad (11)$$

where

$$n_B = n_p + n_n = \sum_N \frac{2k_N^3}{3\pi^2}, \quad N = p, n. \quad (12)$$

is the baryon density.

Finally, the mean field σ is fixed by imposing that

$$\frac{\partial \epsilon}{\partial \sigma} = 0. \quad (13)$$

As mentioned in the Introduction, our interest lies on matter at fixed proton fraction given by $Y_p = n_p/n_B$ as well as in stellar matter in β -equilibrium conditions, which for the system made up of protons, neutrons and electrons are:

$$\mu_p = \mu_n - \mu_e. \quad (14)$$

Model	B/A (MeV)	n_0 (fm ⁻³)	M^*/M	J (MeV)	L_0 (MeV)	K (MeV)
QMC	-15.7	0.150	0.77	34.5	90	295

TABLE I. Nuclear matter bulk properties obtained with the QMC model. All quantities are taken at saturation.

Charge neutrality requires that

$$n_p = n_e. \quad (15)$$

In this article we work with the low density regions of the neutron stars and in this region muons are not present.

III. COEXISTING PHASES APPROXIMATION

In this approximation matter is organized in regions of lower density, generally with a neutron gas in the background and regions of higher density. For a given total density n_B and proton fraction Y_p , the pasta structures are built with different geometrical forms. The forms are usually called: sphere (bubble), cylinder (tube), and slab, in three, two, and one dimensions, respectively. This is achieved by calculating the density and the proton fraction of the pasta and of the background gas from the Gibbs conditions, that impose that both phases have the same pressure and proton and neutron chemical potentials, so that the following equations must be solved simultaneously:

$$P^I = P^{II}, \quad (16)$$

$$\mu_p^I = \mu_p^{II}, \quad (17)$$

$$\mu_n^I = \mu_n^{II}, \quad (18)$$

$$n_p = n_B Y_p = f n_p^I + (1 - f) n_p^{II}, \quad (19)$$

where I (II) label the high-(low-)density phase, n_p is the global proton density, f is the volume fraction of phase I ,

$$f = \frac{n_B - n_B^{II}}{n_B^I - n_B^{II}}. \quad (20)$$

If stellar matter is considered, the above equations are slightly altered in such a way that:

$$\mu_n^I = \mu_n^{II}, \quad (21)$$

$$\mu_e^I = \mu_e^{II} \quad (22)$$

and

$$f(n_p^I - n_e^I) + (1 - f)(n_p^{II} - n_e^{II}) = 0. \quad (23)$$

along with eq. (16). Here the density of electrons is no longer uniform as in the fixed proton fraction case. It appears as the solution of the above equation.

After the lowest energy state is achieved, the surface and Coulomb terms are added to the total energy density of the system, which is given by

$$\varepsilon = f\varepsilon^I + (1 - f)\varepsilon^{II} + \varepsilon_e + \varepsilon_{surf} + \varepsilon_{Coul}. \quad (24)$$

By minimizing the sum $\varepsilon_{surf} + \varepsilon_{Coul}$ with respect to the size of the droplet/bubble, rod/tube or slab we get [6] $\varepsilon_{surf} = 2\varepsilon_{Coul}$ where

$$\varepsilon_{Coul} = \frac{2\alpha}{4^{2/3}} (e^2 \pi \Phi)^{1/3} [\mathcal{S} D (n_p^I - n_p^{II})]^{2/3}, \quad (25)$$

where $\alpha = f$ for droplets, rods and slabs, and $\alpha = 1 - f$ for tubes and bubbles. \mathcal{S} is the surface tension discussed in the next subsection and Φ is given by

$$\Phi = \begin{cases} \left(\frac{2-D\alpha^{1-2/D}}{D-2} + \alpha \right) \frac{1}{D+2}, & D = 1, 3 \\ \frac{\alpha-1-\ln\alpha}{D+2}, & D = 2 \end{cases}. \quad (26)$$

As we are treating only the low density region, the nucleon effective mass M_N^* can be parametrized as

$$M_N^* = M_N - g_{\sigma N}(\sigma)\sigma \quad (27)$$

with

$$g_{\sigma N}(\sigma) = \left(1 + \frac{b}{2}\sigma + \frac{c}{3}\sigma^2\right)g_{\sigma N} \quad (28)$$

where $g_{\sigma N} = 3g_{\sigma}^2 S_N(0) = 8.6157$, $b = 0.000722089$ MeV⁻¹ and $c = 1.17509 \times 10^{-7}$ MeV⁻². Notice that these values are valid only for this specific parameterization.

Before we proceed to the discussion of the surface tension coefficient, it is important to point out that the co-existence phase (CP) method does not take into account the Coulomb interaction and finite-size effects in a self-consistent way. An alternative prescription within the compressible liquid drop (CLD) model incorporates these important effects by minimizing the total free energy, where surface and Coulomb terms are explicitly included [34] self-consistently. The resulting pressure and proton chemical potential equilibrium conditions are slightly different from the ones above. The differences between both prescriptions (CP and CLD) can be easily seen in [35] and the resulting pasta properties differ at very low densities [34, 35], generally lower than 10^{-3} fm⁻³ when the matching to the outer crust EoS is performed. As will be shown next, our calculation depends also on a free parameter, that is fitted according to accepted values of the surface tension.

A. The surface tension coefficient

In order to achieve a numerical value for the surface tension coefficient, the geometrical approach introduced in [36] is used next. In [37], this method was used to compute the surface tension in quark matter but recently it was also used to obtain the surface tension coefficient for hadronic matter [25]. The main ideas are also discussed next.

The surface tension coefficient, \mathcal{S} , which measures the energy per unit area necessary to create a planar interface between the two phases is given by

$$\mathcal{S} = \frac{a}{n_g} \sqrt{2\varepsilon_g} \int_{n_1}^{n_2} \sqrt{\Delta\varepsilon} dn, \quad (29)$$

where $n_g = \frac{n_1+n_2}{2}$, $\varepsilon_g = \frac{\varepsilon(n_1)+\varepsilon(n_2)}{2}$ and $\Delta\varepsilon = \varepsilon_{hm} - \varepsilon_{nhm}$ is the difference between the energy density of the homogeneous and the non-homogeneous matter. These energy densities are fitted to a functional form given by $\varepsilon = an^2 + bn + c$, where n_1 and n_2 are the two coexistence baryonic density points. In this geometrical approach, the width of the interface region and the magnitude of \mathcal{S} are controlled by the adjustable parameter a . In [37] the authors used $a = 1/m_\sigma = 0.33$ fm where $m_\sigma = 600$ MeV is the mass of the σ meson, a natural scale for quark matter. As we are treating hadronic matter in the present work, our initial guess was $a = 1/M_N = 0.21$ fm, where $M_N = 939$ MeV is the nucleon mass. Another attempt followed the recipe used to find the surface tension of hadronic matter in [25] with an extended version of the Nambu-Jona-Lasino model, where $a = 0.1$ fm was adopted to reproduce the value of the surface tension coefficient for the NL3 model [38] within a Thomas-Fermi calculation [39]. Our final choice was $a = 0.023$ fm, so that the value $\mathcal{S} = 1.123$ MeV.fm⁻² for $Y_p = 0.5$ was reproduced as in [25, 39, 40]. In Figure 1 we compare the three choices of a in the search for the pasta phases, i.e., $a = 0.023$ fm, $a = 0.1$ fm and $a = 1/M_N = 0.21$ fm, for $Y_p = 0.5$. We can see that there is a larger region of the pasta phase for $a = 0.023$ fm. In fact, for $Y_p = 0.5$ no pasta phases were found with $a = 0.1$ fm, neither with $a = 0.21$ fm. Therefore, we have chosen $a = 0.023$ fm to be used throughout our calculations.

It is important to stress that the surface tension coefficient varies with the isospin for a given value of a . In Table II we show the values of \mathcal{S} for five different proton fractions. In order to obtain the pasta phases in β -equilibrium matter, we fitted this values of \mathcal{S} to a functional of the form $\mathcal{S} = d + ex + fx^2$, with $d = -0.0389543$, $e = 2.45143$ and $f = -0.209076$, where x is the global proton fraction. We note that there are some works where the proton fraction used in the calculation of the surface tension is the one of the denser phase.

Previous works [1, 6, 19, 25, 39, 40] have shown that the surface tension at zero temperature, not only varies with the proton fraction, but present values in between

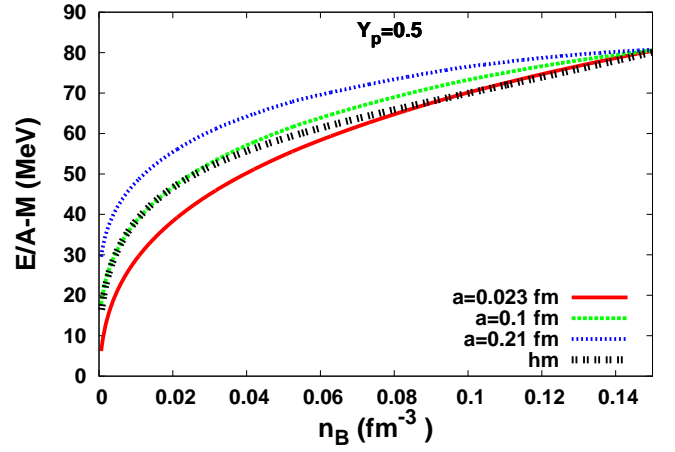


FIG. 1. Energy per baryon as a function of the baryon density proton fraction 0.5 and different choices of a . hm stands for homogeneous npe matter.

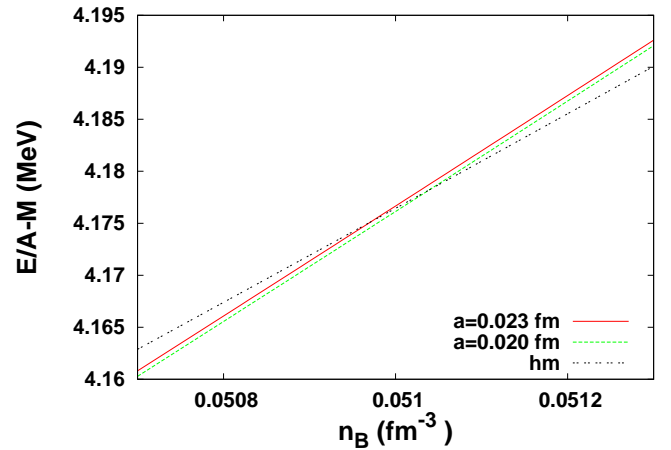
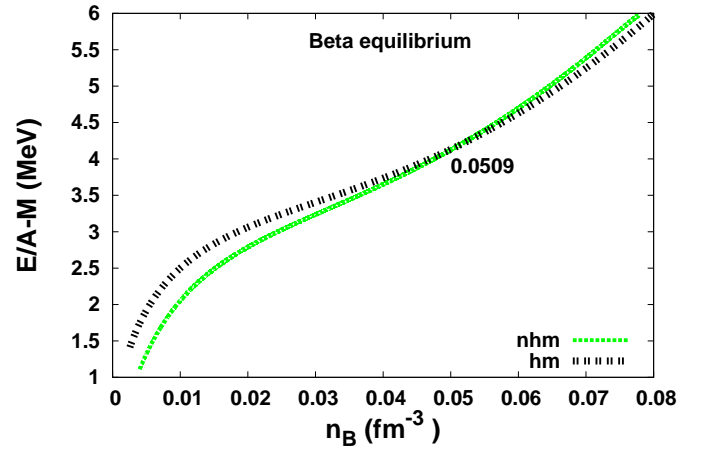


FIG. 2. Free energy per particle obtained for matter in β -equilibrium. The bottom figure shows a zoom of the transition region from the pasta phases to homogeneous matter with two different choices of the parameter a .

Y_p	\mathcal{S} (MeV.fm ⁻²)
0.1	0.21
0.2	0.42
0.3	0.69
0.4	0.93
0.5	1.12

TABLE II. Surface tension coefficient for different proton fractions.

Y_p	\mathcal{S} (MeV.fm ⁻²)	a (fm)	ρ_t (fm ⁻³)
0.5	1.0	0.020	0.100
0.5	1.12	0.023	0.097
0.3	0.60	0.020	0.094
0.3	0.69	0.023	0.093
0.1	0.20	0.020	0.064
0.1	0.21	0.023	0.063
β -eq plot		0.020	0.051
β -eq plot		0.023	0.051

TABLE III. Surface tension coefficient for different proton fractions and related a values. ρ_t is the transition density that separates the pasta from the homogeneous phase.

1.0 and 1.2 MeV.fm⁻² for $Y_p = 0.5$ (see Fig. 5 in [29], for instance). If we constrain the parameter a so that these values are reproduced, we obtain $a = 0.020 - 0.025$ fm. The value $a = 0.020$ fm yields $\mathcal{S} = 1.0$ MeV.fm⁻² and $a = 0.025$ fm results in $\mathcal{S} = 1.2$ MeV.fm⁻² for $Y_p = 0.5$. Choosing $a = 0.025$ would increase the surface energy in 8.7% having a very small effect on the crust-core transition of beta-equilibrium matter. Therefore we proceed with the comparison of the results obtained with $a = 0.020$ and with $a = 0.023$, which entails $\mathcal{S} = 1.123$ MeV.fm⁻² for $Y_p = 0.5$. We then compare our results with those two values of a in Fig. 2, where the free energy per baryon in function of the baryon density for matter in β -equilibrium is shown. We can see that our results are practically independent of a , as far as a reasonable value for the surface tension is used. In Table III we compare the surface tension coefficient \mathcal{S} and the transition density ρ_t for the two values of a . We see that ρ_t is practically independent of a in the range $[0.020, 0.023]$, not only for β -equilibrium matter but also for matter with fixed proton fractions. The surface tension coefficient as a function of the baryon density is displayed in Fig. 3 for matter in β -equilibrium, from where we note that \mathcal{S} decreases with the density. We can see that the surface tension coefficient is only slightly larger for $a = 0.023$ fm both from Table III and Fig. 3.

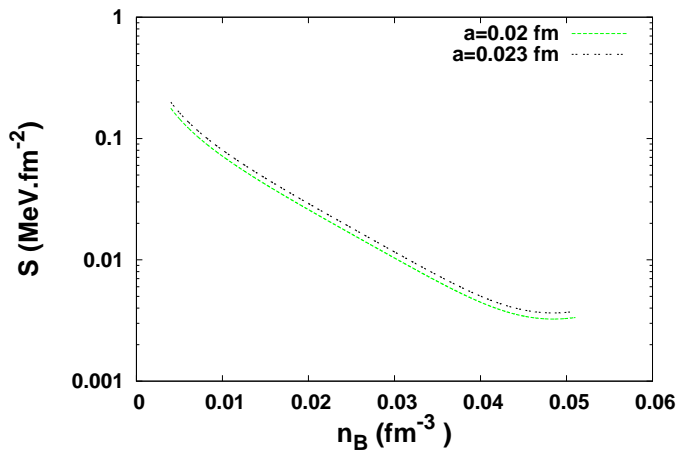


FIG. 3. Surface tension coefficient for β -equilibrium as function of the baryon density for two choices of a .

IV. RESULTS AND CONCLUSIONS

Finally, we present our results for the pasta phases obtained with the QMC model at zero temperature, within the coexisting phases approximation. We would like to remark that pasta is only predicted when its free energy per baryon is lower than the homogeneous npe (neutron-proton-electron) matter.

In Fig. 4 we display the free energy per baryon for $Y_p = 0.5$ and $Y_p = 0.3$. The curves for β -equilibrium matter are shown in Fig. 2. The three cases show the presence of pasta phases, which is bigger for larger proton fractions, as already seen in other works. In Fig. 5 we can see the pasta structures. For $Y_p = 0.5$ three different structures are present: droplets (3D), rods (2D) and slabs (1D), while for $Y_p = 0.3$, a small amount of tubes (2D) also appear. A similar behavior was obtained in [41] for different models. The reason was pointed out to the non-self consistent treatment of the Coulomb force which prevents a redistribution of protons. As a result, the CP method predicts smaller extensions of the pasta phases as a whole and for symmetric matter the larger electron fraction originates stronger Debye screening effects, and therefore, hinders the appearance of tubes.

The pasta phases shrink with the decrease of the proton fraction and for β -equilibrium matter only droplets are present, as predicted in [42] for models with a symmetry energy slope above 80 MeV at saturation density. The transition density between the pasta phases and homogeneous matter shows the same behaviour as in all models, i.e., it decreases for lower proton fraction and the lowest value is obtained for matter in β -equilibrium. The calculations performed in [1] and [19] with the CP method used two different prescriptions for the surface tension coefficient, based on a fitting of the Thomas-Fermi results to a Skyrme and to relativistic models respectively. Apart from these details in the calculations that can

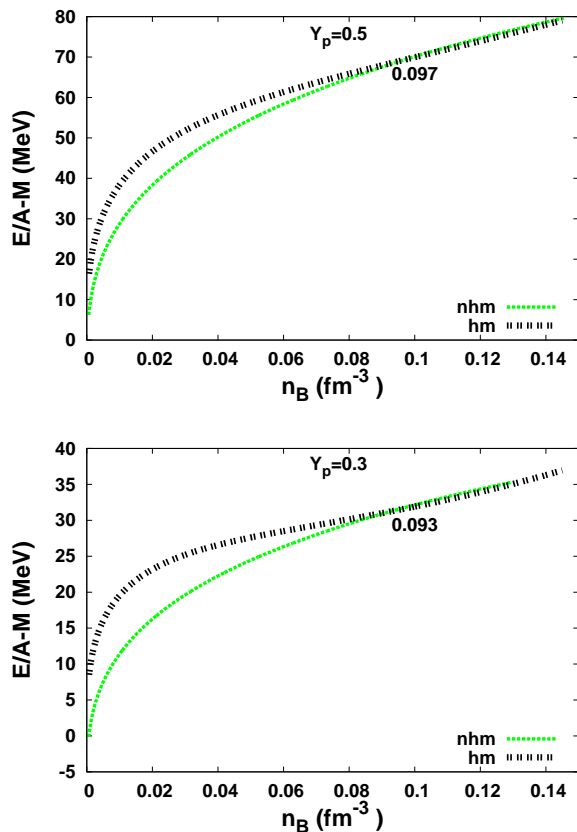


FIG. 4. Free energy per baryon as function of the baryon density with (a) the proton fraction 0.5, (b) proton fraction 0.3 hm=homogeneous matter and nhm=non-homogeneous matter.

modify slightly the quantitative results, the qualitative conclusions do not differ in general.

We note that in Fig. 2 (top) the transition core/crust of a neutron star takes place at $n_B = 0.0509 \text{ fm}^{-3}$. A correlation between the transition densities and the slope has been identified in [19, 43] and in many other works. Since the QMC model has a quite large symmetry energy slope we expect a low crust-core transition density.

Finally, we analyze the influence of the pasta phases on some neutron star properties. In Fig. 6 we show the mass-radius relation. The $M(R)$ curves were built with two equations of state: in one of them (EoS1) we consider the occurrence of pasta, whereas in the other (EoS2) no pasta phases are included. We have used the homogeneous QMC EoS for the core, QMC with pasta and the Baym-Bethe-Pethick (BBP) [44] EoS for the inner crust and the Baym-Pethick-Sutherland (BPS) [45] EoS for the outer crust. In EoS1 the BPS + BBP EoS goes up to $n_B = 1.3 \times 10^{-3} \text{ fm}^{-3}$, the pasta phases lie in between $n_B = 0.15 - 5.05 \times 10^{-2} \text{ fm}^{-3}$ when the core EoS takes on. We match the BPS + BBP EoS directly to the core EoS for densities below $8.9 \times 10^{-3} \text{ fm}^{-3}$ for EoS2. Note that the maximum mass does not change upon the existence of the pasta phases, and both cases reproduce

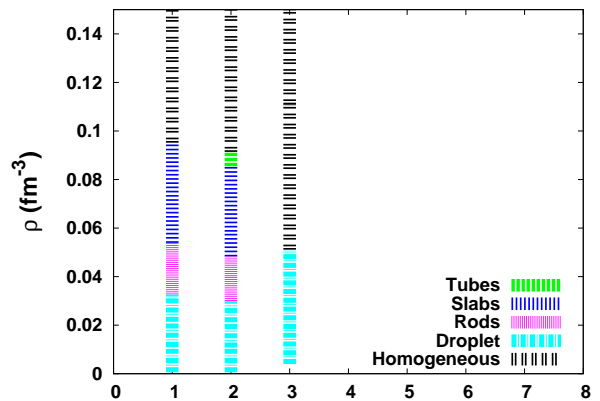


FIG. 5. Phase diagrams at $T=0$ obtained with CP approximation for 1: $Y_p = 0.5$, 2: $Y_p = 0.3$ and 3: β -equilibrium.

$M_{max} = 2.16 M_{sun}$, satisfying the constraints imposed by the recent measurements of the $2M_{sun}$ pulsars PSR J16142230 and PSR J0348+0432 [46, 47] represented by a horizontal black line in the graphic. One of the differences between the results obtained with the two EoS (with and without the pasta phases) appears when we compare the radius of a typical 1.4 solar masses neutron star. The radius when the pasta phase is included is 13.8 km, therefore 600 m smaller than the 14.4 km radius obtained with the BPS+BBP+homogeneous EoS. Hence, only the EoS with pasta phases is inside the radius range proposed in [48], where the authors constrained the canonical $1.4 M_{sun}$ neutron star radii to $R = 9.7 - 13.9$ km, or the radius range obtained in [49] for X-ray bursting NS. However, it is outside the range determined in [50] from the analysis of spectroscopic radius measurements during thermonuclear bursts or in quiescence or in [51] from experimental constraints and causality restrictions. In [52, 53] the authors have also shown the sensitivity of the radius of stars with a mass $\sim 1.4 M_{\odot}$ or lower to the crust EoS and the matching scheme adopted.

V. FINAL REMARKS

In the present work we have revisited the calculation of the pasta phases now using a model with quark degrees of freedom, the QMC model. The determination of the inhomogeneous phases was possible by parameterizing the effective nucleon mass as a non-linear function of the σ meson as done before in [54]. Part of the results shown in the present work will take part in a more comprehensive EoS grid that is being built for star cooling and supernova simulations.

Our results depend quantitatively on a parameter necessary for the calculation of the surface tensor coefficient. We have fitted this parameter to the nuclear surface energy and showed that even changing it in a broad interval the pasta extension was only slightly affected.

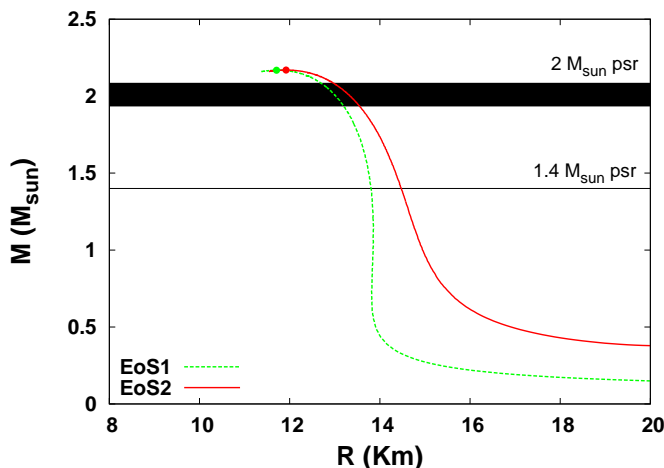


FIG. 6. Mass-radius relation for a family of neutron stars described with the QMC model with (EoS1) and without (EoS2) the pasta phases. The thick horizontal line represents the $2.01 \pm 0.04 M_{\text{sun}}$ pulsar PSR J0348+0432 [47].

The general conclusions related to the size of the pasta

phases, its internal structure and the transition density from the pasta to homogeneous matter go in line with the ones obtained in previous works [1, 19].

Calculations that consider $\omega - \rho$ interaction as the ones performed in [29–31] are currently under investigation with the QMC so that its effect on the pasta phase structure is checked. We intend to incorporate finite size effects through the implementation of the CLD prescription [34, 35] as well. The CLD presents smaller discontinuities at very low densities, so it can be a useful treatment to obtain all the values that will be needed for a complete EoS grid. The inclusion of α particles [39] and other light clusters [40] can also slightly modify the internal structure of the pasta phases.

ACKNOWLEDGMENTS

D.P.M. (grant 300602/2009-0) and G. Grams (doctorate scholarship) acknowledge support from CNPq and Capes. C.P. acknowledges partial support from “New-CompStar”, COST Action MP1304.

-
- [1] S. S. Avancini, D. P. Menezes, M. D. Alloy, J. R. Marinelli, M. M. W. Moraes, and C. Providência, *Phys. Rev. C* **78**, 015802 (2008).
 - [2] J. Xu, L. Chen, B. Li, and H. Ma, *arXiv:0807.4477v3 nucl-ph*, 1 (2009).
 - [3] D. G. Ravenhall, C. J. Pethick, and J. R. Wilson, *Phys. Rev. Lett.* **50**, 2066 (1983).
 - [4] C. J. Horowitz, M. A. Pérez-García, and J. Piekarewicz, *Phys. Rev. C* **69**, 045804 (2004).
 - [5] C. J. Horowitz, M. A. Pérez-García, D. K. Berry, and J. Piekarewicz, *Phys. Rev. C* **72**, 035801 (2005).
 - [6] T. Maruyama et al., *Phys. Rev. C* **72**, 015802 (2005).
 - [7] C. J. Pethick and A. Y. Potekhin, *Phys. Lett. B* **427**, 7 (1998).
 - [8] C. Bertulani and J. Piekarewicz, *Neutron Star Crust* (Nova Science Publishers, Inc., 2012) p. 337.
 - [9] B. Link, R. I. Epstein, and J. M. Lattimer, *Phys. Rev. Lett.* **83**, 3362 (1999).
 - [10] M. D. Alloy and D. P. Menezes, *Phys. Rev. C* **83**, 035803 (2011).
 - [11] U. Furtado, S. Avancini, J. Marinelli, W. Martarello, and C. Providência, *Eur. Phys. J. A* **52**, 290 (2016).
 - [12] H. Shen et al., *Nucl. Phys. A* **637**, 435 (1998).
 - [13] H. Shen et al., *Astrophys. J. Suppl.* **197**, 20 (2011).
 - [14] M. Hempel et al., *Astrophys. J.* **748**, 70 (2012).
 - [15] A. W. Steiner, M. Hempel, and T. Fischer, *Astrophys. J.* **774**, 17 (2013).
 - [16] S. Banik, M. Hempel, and D. Bandyopadhyay, *The Astrophysical J. Supplement S.* **214**, 22 (2014).
 - [17] H. Sonoda, G. Watanabe, K. Sato, T. Takiwaki, K. Yasuoka, and T. Ebisuzaki, *Phys. Rev. C* **75**, 042801 (2007).
 - [18] H. Sonoda, G. Watanabe, K. Sato, K. Yasuoka, and T. Ebisuzaki, *Phys. Rev. C* **77**, 035806 (2008).
 - [19] S. S. Avancini, L. Brito, J. R. Marinelli, D. P. Menezes, M. M. W. de Moraes, C. Providência, and A. M. Santos, *Phys. Rev. C* **79**, 035804 (2009).
 - [20] G. Watanabe, H. Sonoda, T. Maruyama, K. Sato, K. Yasuoka, and T. Ebisuzaki, *Phys. Rev. Lett.* **103**, 121101 (2009).
 - [21] H. Pais and J. R. Stone, *Phys. Rev. Lett.* **109**, 151101 (2012).
 - [22] P. A. M. Guichon, *Phys. Lett. B* **200**, 235 (1988).
 - [23] K. Saito and A. W. Thomas, *Phys. Lett. B* **327**, 9 (1994).
 - [24] K. Saito and A. W. Thomas, *Phys. Rev. C* **52**, 2789 (1995).
 - [25] H. Pais, D. P. Menezes, and C. Providência, *Phys. Rev. C* **93**, 065805 (2016).
 - [26] G. Grams, A. M. Santos, and D. P. Menezes, *Braz. J. Phys.* **46**, 111 (2016).
 - [27] A. M. Santos and C. Providência, *Phys. Rev. C* **79**, 045805 (2009).
 - [28] M. Dutra et al., *Phys. Rev. C* **90**, 055203 (2014).
 - [29] C. Providência et al., *Eur. Phys. J. A* **50**, 44 (2014).
 - [30] D. P. M. Prafulla K. Panda, Alexandre M.S. Santos and C. Providência, *Phys. Rev. C* **85**, 055802 (2012).
 - [31] D. P. M. Rafael Cavagnoli and C. Providência, *Phys. Rev. C* **84**, 065810 (2011).
 - [32] N. Barik, R. N. Mishra, D. K. Mohanty, P. K. Panda, and T. Frederico, *Phys. Rev. C* **88**, 015206 (2013).
 - [33] R. N. Mishra, H. S. Sahoo, P. K. Panda, N. Barik, and T. Frederico, *Phys. Rev. C* **92**, 045203 (2015).
 - [34] S. Bao, J. Hu, Z. Z.W., and S. H., *Phys. Rev. C* **90**, 045802 (2014).
 - [35] H. Pais, S. Chiacchiera, and C. Providência, *Phys. Rev. C* **91**.
 - [36] J. Randrup, *Phys. Rev. C* **79**, 054911 (2009).

- [37] M. B. Pinto, V. Koch, and J. Randrup, *Phys. Rev. C* **86**, 025203 (2012).
- [38] G. A. Lalazissis, J. König, and P. Ring, *Phys. Rev. C* **55**, 540 (1997).
- [39] S. S. Avancini, C. C. Barros, D. P. Menezes, and C. Providência, *Phys. Rev. C* **82**, 025808 (2010).
- [40] S. S. Avancini, C. C. Barros, L. Brito, S. Chiacchiera, D. P. Menezes, and C. Providência, *Phys. Rev. C* **85**, 035806 (2012).
- [41] S. S. Avancini, S. Chiacchiera, D. P. Menezes, and C. Providência, *Phys. Rev. C* **82**, 055807 (2010).
- [42] K. Oyamatsu and K. Iida, *Phys. Rev. C* **75**, 015801 (2007).
- [43] I. Vidana, C. Providencia, A. Polls, and A. Rios, *Phys. Rev. C* **80**, 045806 (2009).
- [44] G. Baym, H. A. Bethe, and C. J. Pethick, *Nucl. Phys. A* **175**, 225 (1971).
- [45] G. Baym, C. Pethick, and P. Sutherland, *Astrophys. J.* **170**, 299 (1971).
- [46] P. Demorest et al., *Nature* **467**, 1081 (2010).
- [47] J. Antoniadis et al., *Science* **340**, 6131 (2013).
- [48] K. Hebeler, J. M. Lattimer, C. J. Pethick, and A. Schwenk, *Phys. Rev. Lett.* **105**, 161102 (2010).
- [49] V. F. Suleimanov, J. Poutanen, D. Klochkov, and K. Wener, *Eur. Phys. J. A* **52**, 20 (2016).
- [50] F. Ozel, D. Psaltis, T. Guver, G. Baym, C. Heinke, and S. Guillot, *Astrophys. J* **820**, 28 (2016).
- [51] A. W. Steiner, J. M. Lattimer, and E. Brown, *Eur. Phys. J* **52**, 18 (2016).
- [52] H. Pais and C. Providencia, *Phys. Rev. C* **94**, 015808 (2016).
- [53] M. Fortin, C. Providência, A. R. Raduta, F. Gulminelli, J. L. Zdunik, P. Haensel, and M. Bejger, *Phys. Rev. C* **94**, 035804 (2016).
- [54] P. A. M. Guichon et al., *Nucl. Phys. A* **601**, 349 (1996).